GEOPHYSICAL RESEARCH LETTERS, VOL. 35, L24803, doi:10.1029/2008GL035866, 2008

Effects of microphysical drop size distribution on tornadogenesis in supercell thunderstorms

Nathan Snook[1] and Ming Xue[1]

Received 31 August 2008; revised 9 November 2008; accepted 18 November 2008; published 20 December 2008.

[1] Idealized simulations of tornadogenesis in supercell storms are performed using a grid of 100 m spacing. The cold pool intensity and low-level storm dynamics are found to be very sensitive to the intercept parameters of rain and hail drop size distributions (DSD). DSDs favoring smaller (larger) hydrometeors result in stronger (weaker) cold pools due to enhanced (reduced) evaporative cooling/melting over a larger (smaller) geographic region. Sustained tornadic circulations of EF2 intensity are produced in two of the simulations with relatively weak cold pools. When the cold pool is strong, the updraft is tilted rearward by the strong, surging gust front, causing a disconnect between low-level circulation centers near gust front and the mid-level mesocyclone. Weaker cold pool cases have strong, sustained, vertical updrafts positioned near and above the low-level circulation centers, providing strong dynamic lifting and vertical stretching to the low-level parcels and favoring tornadogenesis. **Citation:** Snook, N., and M. Xue (2008), Effects of microphysical drop size distribution on tornadogenesis in supercell thunderstorms, *Geophys. Res. Lett.*, *35*, L24803, doi:10.1029/2008GL035866.

1. Introduction

[2] For convective-scale data assimilation and prediction, one of the largest sources of model uncertainty is the microphysical parameterization. Commonly used bulk schemes assume set forms of particle or drop size distributions (DSD). Previous studies [e.g., *Gilmore et al.*, 2004; *van den Heever and Cotton*, 2004] (hereinafter referred to as HC04) demonstrate that the structure, dynamics, and evolution of simulated convective systems are highly sensitive to microphysical (MP) parameterizations. *Gilmore et al.* [2004] showed that variations in DSD-related MP parameters within the observed range of uncertainty can cause significant changes in hydrometeor concentration and type, and precipitation amount and intensity in simulated supercell storms, while HC04 showed that similar variations can change the storm between high-precipitation and low-precipitation types. Both studies used 1 km horizontal grid spacing, insufficient to explicitly predict tornadogenesis. In this study, we perform a set of numerical simulations of supercell storms using a horizontal grid spacing of 100 m. We vary DSD-related parameters within an ice MP scheme to, for the first time, examine the sensitivity of tornadogenesis to these parameters. We also explain the associated dynamics.

2. Numerical Model and Experimental Design

[3] The Advanced Regional Prediction System (ARPS) [*Xue et al.*, 2003], used in this study, is a compressible, nonhydrostatic model suitable for storm-scale simulation and prediction. Mixing ratios of water vapor, cloud water, cloud ice, rain, snow, and hail/graupel are predicted via a commonly used [e.g., *Xue et al.*, 2003; *Hong and Lim*, 2006] Lin-type single moment MP scheme [*Lin et al.*, 1983] (hereinafter referred to as LF083). An exponential DSD is assumed for hydrometeor species: $n_x(D) = n_0 x \exp(-\lambda_x D_x)$, where λ is the slope parameter and n_0 the intercept parameter. $n_x(D)\delta D$ represents the number of hydrometeors per unit volume with diameter between D and $D + \delta D$, and x denotes the hydrometeor species (rain, snow, or hail/graupel). The slope parameter can be expressed as a function of the intercept parameter, density, and mixing ratio of the species. Cloud water and cloud ice are assumed to be monodisperse. Single-moment MP schemes like those of LF083 predict the mixing ratios and specify intercept parameters as constant values.

[4] Intercept parameters for rain, hail, and snow DSDs vary widely in nature. Intense convection typically yields DSDs favoring large raindrops, while stratiform rain DSDs tend to favor small raindrops. Hail DSDs are even more variable, with some storms producing only small hailstones/graupel (or none at all) and other storms producing many hailstones greater than 10 cm in diameter. Observational studies have yielded values of rain and hail intercept parameters spanning two to four orders of magnitude [*Waldvogel*, 1974; *Lo and Passarelli*, 1982]. With such a wide range of observed values, it is vital to obtain a better understanding of model sensitivity to these parameters.

[5] The storm environment for this study is defined by a sounding associated with the May 20, 1977, Del City, Oklahoma storm [*Ray et al.*, 1981] with a mean storm motion vector of (3, 14) m s^{-1} subtracted. Free-slip lower boundary and radiative lateral boundary conditions are used. Initial convection is triggered by a low-level thermal bubble of 4 K maximum perturbation, with vertical and horizontal radii of 1.5 and 5 km, respectively. Existing studies that attempt to simulate tornadoes within supercell storms usually employ nested grids [e.g., *Grasso and Cotton*, 1995]. In this study, we employ a uniform horizontal grid spacing of 100 allowing the model to freely develop tornadoes. Only rain and hail DSDs are varied because they have the strongest influence on cold pool intensity, defined in terms of temperature perturbation [*Snook and Xue*, 2006]. Table 1 lists the configurations of all experiments presented.

[1] School of Meteorology and Center for Analysis and Prediction of Storms, University of Oklahoma, Norman, Oklahoma, USA.

0094-8276/08/2008GL035866$05.00

Table 1. Summary of Experiments

Experiment Name	Intercept Parameter			Characteristics
	Rain	Hail	Snow	
CNTL	8×10^6	4×10^4	8×10^6	Control
H2	8×10^6	4×10^2	8×10^6	Large hailstones
H6	8×10^6	4×10^6	8×10^6	Small hailstones
R5	8×10^5	4×10^4	8×10^6	Large raindrops
R7	8×10^7	4×10^4	8×10^6	Small raindrops
H2R5	8×10^5	4×10^2	8×10^6	Large hailstones and raindrops
H6R7	8×10^7	4×10^6	8×10^6	Small hailstones and raindrops

The control intercept parameter values are the default in the work by LF083 while other values are chosen within the observed range. A domain of $64 \times 64 \times 16$ km^3 is used with 81 vertical levels; vertical grid spacing increases from 20 m near the ground to roughly 400 m at the model top.

3. Results

3.1. General Storm Evolution

[6] Major differences quickly develop between the seven simulations performed (Table 1). Simulations where DSDs favor larger hydrometeors (H2, R5, H2R5) result in relatively weak cold pools, leading to the formation of single or multiple supercells with steady updrafts (Figure 1a). Supercells are also present in simulations with moderate to strong cold pools (CNTL, H6, R7), though these supercells are cyclic in nature, with multiple updraft pulses. This agrees with the results of HC04 regarding the effect hail DSD variation on supercell cycling. In the two simulations that result in the most intense cold pools (R7 and H6R7), supercells are present initially but the system later transitions to a more linear mode (Figure 1b) due to the strong linear forcing of the gust front.

3.2. Microphysical Effects

[7] To further explore the cold pool dynamics, budget analyses are performed on the MP conversion terms. The total mass converted from one species to another is calculated at each time step and multiplied by the corresponding latent heat (of fusion, vaporization, or sublimation) to yield net cooling/heating. To focus on cold pool effects, budget calculations are limited to downdraft regions below 5 km above ground level where vertical velocity w is less than -0.5 m s^{-1} and performed between 3600 and 7200 s, during which period the cold pool develops to maturity.

[8] Two MP processes are found to be dominant in cooling contribution. The largest contribution comes from evaporation of rain, and the second largest from melting of hail/graupel. Time series of these terms are shown in Figure 2. The ratio of the cooling contribution of hail/graupel melting to that of rain evaporation (not shown) ranges from approximately 0.1 in H6R7 to approximately 0.55 in R5. Contributions from other conversion terms are more than an order of magnitude smaller.

[9] The amount of cooling due to rain evaporation differs significantly among the experiments. When the total integrated cooling within the defined downdraft region is normalized by that of CNTL (see Figure 2, left), the contributions from rain evaporation range from 0.25 in H2R5 to 2.28 in H6R7. Evaporative cooling in H2 and R5 is only about half of that in CNTL. Conversely, H6 and R7 show about 50% more evaporative cooling. Larger raindrops fall faster, limiting the areal extent of precipitation and evaporative cooling. More importantly, few larger raindrops have less total surface area than many smaller ones containing the same amount of water, also resulting in less evaporation and cooling. The net result is a smaller, weaker cold pool.

[10] Variation of the cooling contribution from melting of hail/graupel is much less pronounced among the runs. The ratios to that of CNTL range between 0.82 and 0.9 for R5, R7, H6, and H6R7, and are equal to 0.48 and 0.35 in H2 and H2R5, respectively (Figure 2, right). Relatively little change in the melting cooling is introduced by varying the rain DSD (curves for R5 and R7 in the right plot of Figure 2). The only significant departures from CNTL are in H2 and H2R5 that favor larger hailstones, where melting is reduced by decreased surface area. Variation of the hail intercept parameter has a stronger indirect influence on cold pool intensity by changing the distribution and intensity of rainfall than it does any direct influence on cold pool intensity.

3.3. Tornadic Activity

[11] Sustained tornadic vortices are observed in two simulations: CNTL and R5, as noted in Figure 3, which shows the time series of maximum low-level (<2 km level) vertical cyclonic vorticity from CNTL, R5, R7, and H6R7. The tornadic vortex in CNTL lasts approximately four minutes beginning at 13200 s, with a maximum low-level wind speed of 55 m s^{-1}, corresponding to a EF2 intensity. The near-surface vortex in R5 lasts approximately 10 minutes beginning at 12000 s, with a maximum surface wind speed of 58 m s^{-1} (also EF2 intensity).

[12] CNTL and R5 feature well-defined supercells with weak to moderately intense cold pools. In H6R7 and R7, cold pools are very strong and surface vortices are weak and short lived. The physical effects of cold pool intensity on storm dynamics and tornadogenesis can be elucidated by examining vertical cross-sections through the updraft cores. Such cross-sections are shown for R5 and H6R7, which have weak and strong cold pools, respectively (Figures 1a and 1d). They suggest that the strength of the gust front is a key factor in determining updraft orientation, in a similar way as in squall lines [*Rotunno et al.*, 1988]. In simulations with weaker cold pools, the gust front is positioned beneath or just ahead of the mid-level updraft core; a balance between the cold pool and the gust-front-relative inflow supports an intense, erect updraft.

[13] Figures 1b and 1c show the time-dependent trajectories of five representative low-level parcels entering the updraft core in R5. These parcels are released at such times that they would enter a mature cell near its peak intensity. In R5, the parcels released near the surface in the inflow region initially travel southwestward and remain near the surface until turning upward at the gust front. They then rise with a moderate westward slope to mid-levels (between 1.5 to 4 km) before moving into a deep vertical updraft that extends to 14 km level (Figures 1b and 1c).

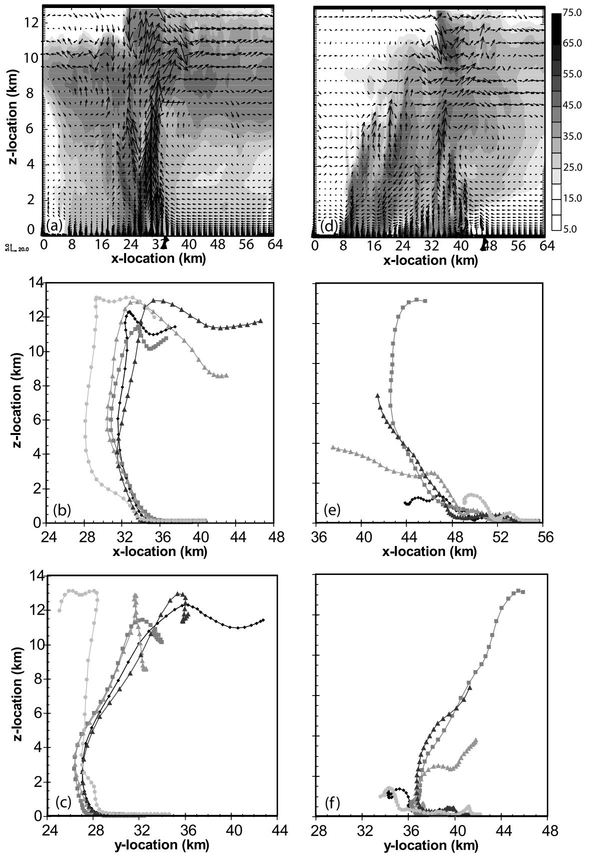

Figure 1. The x-z cross-sections of radar reflectivity (shaded) and wind vectors for (a) R5 and (d) H6R7 taken through locations of maximum updraft intensity, and trajectories in the (b and c) x-z and (e and f) y-z planes of five parcels initially located within the inflow region of the storms in R5 (Figures 1b and 1c) and H6R7 (Figures 1e and 1f). Points along the trajectories are separated by 30 seconds. In R5, tornadogenesis occurs about 20 min after trajectory initialization while in H6R7 tornadogenesis does not occur.

[14] In simulations with stronger cold pools, the gust front quickly races ahead relative to the mid-level updraft core and (potential) mesocyclone circulation, often by several kilometers (Figure 1d). The result is a weaker, strongly sloping updraft, often with multiple updraft "pulses", promoting cyclic behavior or in extreme cases (having particularly strong cold pool and gust front) a linear, non-supercellular storm mode. When low-level inflow parcels are tracked for H6R7 (Figures 1e and 1f), they also begin by traveling southwestward near the surface. However, upon encountering the gust front and entering the updraft, they maintain strongly rearward-sloping trajectories up to the mid-levels, resulting a significant horizontal separation between potential low-level vorticity centers forming near the gust front and the mid-level updraft and mesocyclone (given streamwise vorticity in the updraft inflow).

[15] The low-level tornadic circulation in R5 is located much closer horizontally to its parent mesocyclone than that in CNTL, corresponding to the differences in vertical structure noted above. Mesocyclone and tornado locations at the times of peak tornado intensity in CNTL and R5 are shown in Figures 4a and 4b, respectively. In CNTL, the tornado (marked "T") is located approximately 8 km east of the center of the mesocyclone (marked "M"). The tornado in R5 is located just 3 km northeast of the mesocyclone center. Figure 4c shows low-level fields in a zoomed-in region in the inset box of Figure 4b. The strong tornadic vortex is found just behind the gust front, near the tip of the occluding forward-flank and rearward-flank gust fronts, almost directly below the mid-level mesocyclone and intense updraft. With such positioning, the dynamic upward pressure gradient forcing induced by the mesocyclone and the suction effect of the overlying buoyant updraft act to produce strong vertical stretching at the lower levels, promoting tornadogenesis [*Klemp*, 1987]. This is supported by our preliminary diagnostic analyses of force and vorticity components (to be reported elsewhere) along the trajectories of parcels passing through the tornado vortex. Trajectory analyses reveal that the air parcels feeding the tornado vortex come from the cold side of the gust front; they originate at near 1.5 km AGL ahead of the storm (from the east), descend to the ground in the rear-flank downdraft, then flow towards the gust front where they are forced upward by surface convergence and dynamic lifting (Figure 4d). Such complete trajectory paths and associated behaviors have not been explicitly documented in previously published studies; they further indicate the relevance of cooling within the downdraft region to parcel buoyancy and gust front propagation, and the importance of lifting to such cold-pool air by a different branch of flow: the updraft and associated mesocyclone. The role of downdraft air to tornadogenesis is also investigated in a study by *Davies-Jones* [2008] which focuses on a somewhat different mechanism.

[16] Our results are consistent with the observational findings of *Markowski et al.* [2002] that "relatively cold, stable surface air parcels were found to be more widespread in nontornadic RFDs (rear flank downdrafts)" and "tornado likelihood, intensity, and longevity increase as the surface buoyancy, potential buoyancy (CAPE), and equivalent potential temperature in the RFD increase". Our results also agree with *Markowski et al.* [2003] who found that relatively warm downdrafts resulted in stronger, longer-lived tornadoes in an idealized axisymmetric tornado model with prescribed rain-cooled downdraft. *Lerach et al.* [2008] also found increasing aerosol concentrations within a supercell environment yields a reduction in cold- and warm-rain

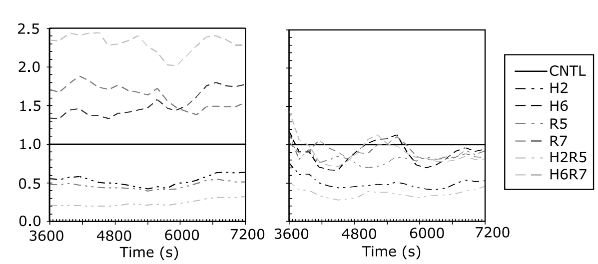

Figure 2. Contributions of evaporation of (left) rainwater and melting of (right) graupel to cold pool cooling relative to those in CNTL (unitless ratios). The contributions were integrated totals in downdraft regions below z = 5 km where $w < -0.5$ m s^{-1}.

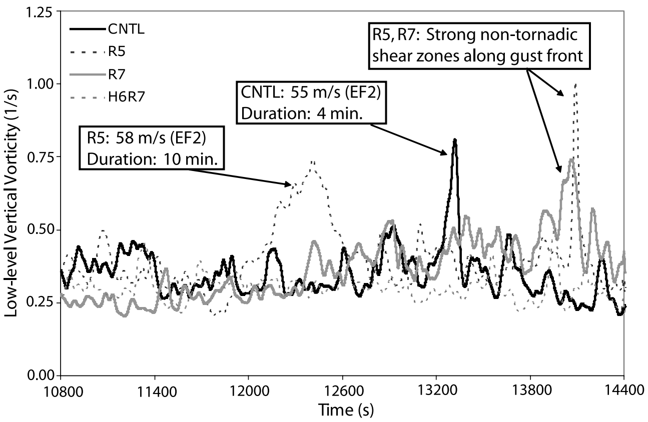

Figure 3. Time series of maximum low-level (below 2 km) cyclonic vertical vorticity for tornadic cases CNTL and R5 (black lines), and non-tornadic cases R7 and H6R7 (gray lines). A 30-second running average was applied. Prominent vorticity maxima (both tornadic and non-tornadic) are noted, along with duration and intensity on the Enhanced Fujita scale (if applicable), from 3 to 4 hours of model time.

MP processes and results in a weaker cold pool and conditions more favorable for tornadic development.

4. Summary

[17] Numerical simulations of a supercell storm are found to be highly sensitive to variations in MP DSD parameters. Varying only the intercept parameters of rain and/or hail DSDs within their typical uncertainty range yields solutions ranging from single to multiple supercell formation to linear convection. When the DSD parameters favor larger (smaller) hydrometeors, weaker (stronger) cold pools result. The reduction in total hydrometeor surface area associated with larger raindrops/hailstones leads to less evaporation and melting, which are the dominant processes affecting the cold pool intensity. In addition, the faster-falling larger hydrometeors reduce the areal coverage of precipitation and the coverage and intensity of the cold pool.

[18] These results, obtained at a 100 m horizontal resolution, show that the rain and hail DSD parameters have a strong influence on tornadogenesis through their effects on the cold pool. Tornadogenesis potential is greater when

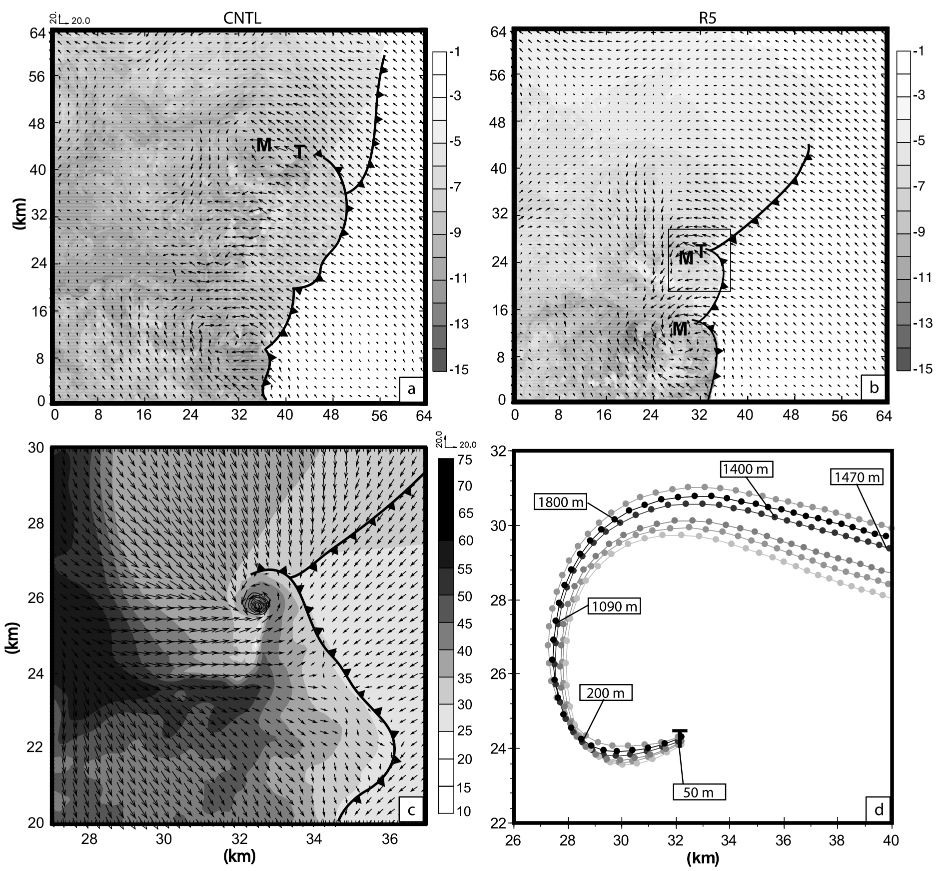

Figure 4. Comparison of (a) CNTL and (b) R5 at the time of peak tornado intensity. Plotted are perturbation potential temperature at the surface (shaded, K) and winds at 2500 m AGL (vectors, m s^{-1}). Locations of mid-level mesocyclones and low-level tornadoes are labeled 'M' and 'T', respectively, gust front position is indicated by the thick black lines. (c) Reflectivity (shaded), vertical vorticity (contour), and wind vectors 10 m AGL from R5, in the boxed region in Figure 4b. (d) Trajectories of air parcels, projected onto the x-y plane, prior to entering the tornado vortex in R5 (marked 'T') shortly after tornadogenesis. Height of selected parcels above ground level is shown.

there is a near-vertical alignment between low- and mid-level vorticity centers and when the air in the downdraft region is warmer (and thus more buoyant). When the cold pool is of proper strength and a balance between the cold pool and low-level inflow exists, vertical, erect, rotating (given a supercell sounding) updrafts form in close proximity to the gust front, providing dynamic lifting to the low-level air whose vertical vorticity can be amplified by orders of magnitude through strong vertical stretching near the surface. In our case, the air parcels that feed the tornadic vortex near the surface are found to be cold-pool air that has earlier descended to the ground in the downdraft region. These parcels are potentially buoyant because they originate from the boundary layer inflow ahead of the storm.

[19] When the cold pool is overly strong, rearward sloping updrafts form, segregating any mid-level cyclone from the low-level gust front where convergence helps to lift cold air. Tornadogenesis potential is greatly reduced without strong upward dynamic forcing and associated vertical stretching. Although strong baroclinity at the gust front can produce strong horizontal vorticity that can be tilted into vertical, the vorticity spin-up tends to be short-lived. The very cold air is also less buoyant and harder to lift.

[20] While the results of this study are robust, cold pool intensity alone cannot predict tornadogenesis or its failure. Supercell tornadogenesis likely requires an optimal balance between cold pool strength and environmental flow, and storm dynamics will certainly be influenced by other parameters such as convective available potential energy (CAPE). Further research efforts will be necessary to gain a more complete understanding of tornadogenesis.

[21] **Acknowledgments.** This work was supported by NSF grants EEC-0313747, ATM-0530814, ATM-0331594 and ATM-0331756 and simulations were performed at the Pittsburgh Supercomputing Center.

References

Davies-Jones, R. (2008), Can a descending rain curtain in a supercell instigate tornadogenesis barotropically?, *J. Atmos. Sci.*, *65*, 2469–2496.

Gilmore, M. S., J. M. Straka, and E. N. Rasmussen (2004), Precipitation uncertainty due to variations in precipitation particle parameters within a simple microphysics scheme, *Mon. Weather Rev.*, *132*, 2610–2627.

Grasso, L. D., and W. R. Cotton (1995), Numerical simulation of a tornado vortex, *J. Atmos. Sci.*, *52*, 1192–1203.

Hong, S.-Y., and J.-O. J. Lim (2006), The WRF single-moment 6-class microphysics scheme (WSM6), *J. Korean Meteorol. Soc.*, *42*, 129–151.

Klemp, J. B. (1987), Dynamics of tornadic thunderstorms, *Annu. Rev. Fluid. Mech.*, *19*, 369–402.

Lerach, D. G., B. J. Gaudet, and W. R. Cotton (2008), Idealized simulations of aerosol influences on tornadogenesis, *Geophys. Res. Lett.*, *35*, L23806, doi:10.1029/2008GL035617.

Lin, Y.-L., R. D. Farley, and H. D. Orville (1983), Bulk parameterization of the snow field in a cloud model, *J. Clim. Appl. Meteorol.*, *22*, 1065–1092.

Lo, K. K., and R. E. Passarelli Jr. (1982), The growth of snow in winter storms: An airborne observational study, *J. Atmos. Sci.*, *39*, 697–706.

Markowski, P. M., J. M. Straka, and E. N. Rasmussen (2002), Direct surface thermodynamic observations within the rear-flank downdrafts of nontornadic and tornadic supercells, *Mon. Weather Rev.*, *130*, 1692–1721.

Markowski, P. M., J. M. Straka, and E. N. Rasmussen (2003), Tornadogenesis resulting from the transport of circulation by a downdraft: Idealized numerical simulations, *J. Atmos. Sci.*, *60*, 795–823.

Ray, P. S., B. Johnson, K. W. Johnson, J. S. Bradberry, J. J. Stephens, K. K. Wagner, R. B. Wilhelmson, and J. B. Klemp (1981), The morphology of severe tornadic storms on 20 May 1977, *J. Atmos. Sci.*, *38*, 1643–1663.

Rotunno, R., J. B. Klemp, and M. L. Weisman (1988), A theory for strong long-lived squall lines, *J. Atmos. Sci.*, *45*, 463–485.

Snook, N., and M. Xue (2006), Sensitivity of tornadogenesis in very-high-resolution numerical simulations to variations in model microphysical parameters, paper presented at 23rd Conference on Severe Local Storms, Am. Meteorol. Soc., St. Louis, Mo.

van den Heever, S. C., and W. R. Cotton (2004), The impact of hail size on simulated supercell storms, *J. Atmos. Sci.*, *61*, 1596–1609.

Waldvogel, A. (1974), The N0 jump of raindrop spectra, *J. Atmos. Sci.*, *31*, 1067–1078.

Xue, M., D.-H. Wang, J.-D. Gao, K. Brewster, and K. K. Droegemeier (2003), The Advanced Regional Prediction System (ARPS), storm-scale numerical weather prediction and data assimilation, *Meteorol. Atmos. Phys.*, *82*, 139–170.

N. Snook and M. Xue, Center for Analysis and Prediction of Storms, University of Oklahoma, 120 David Boren Boulevard, Room 5240, Norman, OK 73072, USA. (mxue@ou.edu)